Colloid Polym Sci (2015) 293:409–420
DOI 10.1007/s00396-014-3400-z

ORIGINAL CONTRIBUTION

Targeted drug delivery potential of hydrogel biocomposites containing partially and thermally reduced graphene oxide and natural polymers prepared via green process

B. A. Aderibigbe · S. J. Owonubi · J. Jayaramudu · E. R. Sadiku · S. S. Ray

Received: 13 May 2014 / Revised: 12 September 2014 / Accepted: 14 September 2014 / Published online: 24 October 2014

Abstract Hydrogel biocomposites containing a combination of partially and thermally reduced graphene oxide (rGO) and natural polymer were prepared by free radical polymerization. The effect of rGO and the natural polymer on the morphology of the hydrogel composites was studied. The 0.007 g of rGO was used for uniform dispersion within the hydrogel composite matrix. The swelling kinetic and swelling ratios of the composites were evaluated at pH 1.2 and 7.4. Drug release studies were performed at pH values of 1.2 and 7.4 simulating gastric juice and intestinal fluid pH, respectively. The hydrogel biocomposites were able to bypass the acidity of the simulated gastric juice without liberating substantial amounts of the loaded drug, suggesting that rGO containing hydrogels are potential targeted drug delivery systems. The hydrogel biocomposites were further characterized by Fourier transform spectroscopy, X-ray diffraction, scanning electron microscopy, transmission electron microscopy, and differential scanning calorimetry.

Keywords Graphene oxide · Targeted drug delivery · Hydrogels biocomposite · Drug release

B. A. Aderibigbe (✉)
Department of Chemistry, University of Fort Hare, Alice Campus, Alice, South Africa
e-mail: blessingderibigbe@gmail.com

S. J. Owonubi · E. R. Sadiku
Department of Chemical, Metallurgical and Material Engineering, Tshwane University of Technology, Pretoria, South Africa

J. Jayaramudu · S. S. Ray
DST/CSIR National Centre for Nanostructured Materials, Council for Scientific and Industrial Research, 0001 Pretoria, South Africa

Introduction

Carbon-based materials are environmentally and biologically friendly. Graphene is a carbon- based material, and it is made up of sp^2 bonded carbon atoms, which are tightly packed in a two-dimensional honeycomb lattice [1–3]. The synthesis of graphene-based materials has attracted a lot of attention because of its outstanding properties, such as excellent electrical conductivity, high mechanical strength, unparalleled thermal conductivity, high energy, high elasticity, high surface area, power densities, and ease of functionalization [4–6]. Their ability to adsorb a variety of aromatic biomolecules through a π–π stacking interaction and electrostatic interaction make them ideal materials for biomedical applications such as drug loading. They are used in several applications, such as composite materials [7, 8], batteries [9, 10], fuel cells [7], capacitors [11], electronics [12], and biosensors [13].

Graphene oxide (GO) has been found to be very useful in biomedical applications because of its unique properties such as high therapeutic loading capacity, high surface area, and negative charge which establish electrostatic interactions with positively charged (i.e., highly hydrophilic) polymers and the presence of variety of functional groups on its surface allows the possibility of versatile surface biconjugation. In a research report by Bai et al. [13], pH-sensitive GO/PVA (polyvinyl alcohol) composite hydrogels were prepared for selective drug release studies at physiological pH. In another report, GO/poly-(nisopropylacrylamide) interpenetrating hydrogels with thermal and pH responses were prepared and used as potential carriers for controlled drug delivery [15]. In another research report, a series of GO/poly (acrylic acid-co-acrylamide) superabsorbent hydrogel nanocomposites were prepared via in situ radical solution polymerization [16]. In the application of rGO for drug delivery, a research by Miao et al.

reported the preparation of cholesteryl hyaluronyl reduced graphene oxide (rGO) nanosheets for tumor-targeting delivery system for doxorubicin [17]. The in vivo antitumor effects was found to be greatest in tumor bearing mice treated with cholesteryl hyaluronic acid-coated rGO containing doxorubicin. In another research report by Wei et al., drug delivery system based on the covalently linked rGO with p-aminobenzoic were prepared for the loading and targeted delivery of doxorubicin. The drug delivery system was found to be pH-dependent [18]. In another research report, the application of rGO in drug delivery was demonstrated, and its effect on the loading and delivery of doxorubicin was investigated, and it was found to enhance the cancer-cell apoptosis effectively [19].

Targeted delivery systems are also referred to as smart delivery systems [20]. These systems prolong a protected drug interaction with the diseased cell or organ. It has been found to exhibit several advantages such as controlled release of the drug at a target organ and reduction of side effect associated with the drug; it minimizes the access of the drug to normal organs, thereby reducing the toxic effects, and the drug concentration to the required organs can be increased without harmful effects on other organs. Different types of delivery carriers used in targeted drug delivery systems are dendrimers [21], liposomes [22], polymeric micelles [23], and biodegradable particles [24]. Presently few drug delivery systems have been developed which have potential for treatment of diabetes [25], cancer [26], heart diseases [27], and rheumatoid arthritis [28].

Whey protein isolate (WPI) is a natural polymer that is protein-based. It is biodegradable, biocompatible, nontoxic, and readily available [29]. These properties make it ideal for the preparation of drug delivery systems. It is used as recombinants in DNA technology [30] and in hydrogels, for inactivation of bacteria [31]. To date, no researcher has reported the combination of rGO, synthetic polymer, and natural polymer in hydrogel biocomposites for targeted drug release mechanism. In this research, hydrogel biocomposites containing WPI and rGO were prepared. The effects of the content of WPI and rGO on the chemical structure, morphology, and drug release mechanism of the hydrogel biocomposites were evaluated. Targeted drug delivery potential of the hydrogel biocomposites was evaluated by performing release studies of 8-aminoquinoline using UV–vis spectroscopy at pH values of 1.2 and 7.4. The hydrogel biocomposites were characterized using Fourier transform infrared spectroscopy (FTIR), X-ray diffraction (XRD), differential scanning calorimetry (DSC), scanning electron microscopy (SEM), and transmission electron microscopy (TEM). The swelling kinetics, swelling behaviors, and pH-responsive behaviors of the biocomposites were evaluated.

Experimental

Materials

Whey protein isolate (WPI) powder was obtained from Honeyville Food Products, Salt Lake City, Utah, USA. It contained 90 % protein, 4 % fat (acid hydrolysis), about 5 % ash, and 1 % other minor constituents. Acrylamide (AM), 8-hydroxyquinoline, *N*, *N*'-methylenebisacrylamide (MBA), potassium persulfate (KPS), and *N*, *N*, *N*, *N*'-tetramethylethylenediamine (TMEDA) were purchased from Sigma Aldrich, South Africa. De-ionized water was used for the preparation of the hydrogels. rGO was donated by J. Jayaramudu research group.

Preparation of the hydrogel biocomposites

The hydrogel biocomposites were prepared by dissolving WPI in (3 mL, 0.05 M) sodium hydroxide solution, followed by the addition of acrylamide (1 g) and MBA solution (1 mL, 0.0648 mM). The mixture was thoroughly stirred in order to obtain a homogenous mixture before the addition TMEDA (1 mL, 86.1 mM), rGO (0.007 g), and KPS (1 mL, 37 mM), respectively (Table 1). The hydrogels were formed at a temperature between 40 and 60 °C. The hydrogel biocomposites were then soaked in distilled water overnight in order to get rid of unreacted amine, before drying at ambient temperature for 3 days (Table 1).

Swelling studies of the hydrogel biocomposites

Swelling kinetics is a very important property in drug delivery systems because it influences the release mechanism of the drug. Dry hydrogel biocomposites (50 mg) were immersed in (25 mL) of selected buffer solution (pH 5.8, 7.4, and 10) at ambient temperature. After pre-determined interval, they were removed and blotted gently with blotting paper in order to remove the excess water on the surface and weighed. The immersion time and drying of the hydrogel biocomposites were repeated until the weight of the swollen hydrogel

Table 1 Percentage loading efficiency and the reaction conditions for the hydrogel biocomposites

Hydrogels biocomposites	WPI (g)	GO (g)	KPS (mL)	AM (g)	MBA (mL)	TMEDA (mL)	Drug loading efficiency (%)
rGO-blank	–	–	1	1	1	1	26±2.8
rGO-1	0.05	–	1	1	1	1	41±1.4
rGO-2	0.05	0.007	1	1	1	1	24±0.71
rGO-3	–	0.007	1	1	1	1	18±1.4

biocomposites were constant after 24 h. The swelling ratio at equilibrium (ESR) of the biocomposites was calculated from Eq. 1:

$$ESR = M_t - M_d / M_d \quad (1)$$

Where M_t is the weight of the hydrogel biocomposite at equilibrium and M_d is the weight of the dried hydrogel biocomposite before swelling.

The swelling ratio (SR) measurements for the hydrogel composites were determined by immersing dry hydrogel biocomposites (50 mg) in (25 mL) of selected buffer solution (pH 5.8, 7.4, and 10) at ambient temperature. After an interval of 30 min, the hydrogel biocomposites were removed from the buffer solution and blotted gently with blotting paper and weighed. SR was calculated from Eq. 2:

$$SR = M_s - M_d / M_d \quad (2)$$

Where M_s is the weight of the hydrogel biocomposite at time t and M_d is the weight of the dried hydrogel biocomposite before swelling.

Drug loading

The content of 8-hydroxyquinoline in the hydrogel biocomposites was determined by placing 50 mg each of dry rGO-blank, rGO-1, rGO-2, and rGO-3 in 8-hydroxyquinoline solution (25 mL, 3 mM) overnight at ambient temperature. The biocomposites were allowed to reach equilibrium swelling in the drug solution at ambient temperature, after which they were removed from the drug solution and rinsed with distilled water in order to remove any excess drug present on the surface of the hydrogels. They were left to dry at room temperature for 4 days. The percentage encapsulation efficiencies (*DE*) was calculated, based on the ratio of amount of 8-hydroxyquinoline encapsulated in the biocomposites to the amount used in the loading process. It was determined by using UV-visible spectroscopy (Perkin Elmer LAMDA 750S UV/VIS Spectrometer) at a wavelength of 308 nm. The percentage encapsulation efficiencies for the hydrogel biocomposites were calculated by using Eq. 3:

$$DE = A_1 / A_2 \times 100\% \quad (3)$$

Where A_1 is the actual amount of 8-hydroxyquinoline loaded on to the biocomposites and A_2 is the theoretical amount of 8-hydroxyquinoline loaded on the biocomposites. The *DE* results are depicted in Table 1.

In vitro release studies

In vitro release mechanism of 8-hydroxyquinoline from the hydrogel biocomposites were studied. The dried 8-hydroxyquinoline encapsulated hydrogel biocomposites were each placed in 30 mL of selected buffer solutions (i.e., pH values of 1.2 and 7.4). A shaker, BS-06 (Lab Companion) was used for the study at 100 rpm and at a temperature of 37 °C. The release profiles of 8-hydroxyquinoline from the biocomposites were obtained using UV-visible spectroscopy at a wavelength of 308 nm. The release study was performed over a period of 24 h by collecting 4 mL of the sample solution and replacing it with equivalent amount of buffer solution. The time interval used for the release study was selected because the hydrogel biocomposites were found to reach equilibrium swelling over a period of 24 h. For the calibration graph, seven standard solutions were prepared by dilution of the corresponding stock solution to obtain a concentration of 3×10^{-6}–3 mM. The cumulative drug release was calculated using Eq. 4.

$$\%\text{Cumulative 8-hydroxy quinoline} = I_i / I_f \times 100 \quad (4)$$

Where I_i and I_f are the initial amount and cumulative amount of 8-hydroxyquinoline released at time.

FTIR

FTIR analysis was used to identify the functional groups present in 8-hydroxyquinoline and the biocomposites and to indicate the presence of 8-hydroxyquinoline in the biocomposites. It was performed using the Perkin Elmer Spectrum 100 FTIR spectrometer (USA), in a range of 4,000–400 cm^{-1}. It was performed on 8-hydroxyquinoline, rGO-blank, rGO-1, rGO-2, and rGO-3 hydrogel biocomposites.

SEM

The surface morphologies were investigated by SEM analysis on 8-hydroxyquinoline and selected hydrogel biocomposites before and after encapsulation with 8-hydroxyquinoline. Dry hydrogel biocomposites were sputtered with gold nanoparticle before SEM analysis was performed on a JEOL-JSM 7500 F Scanning Electron Microscope, USA, at an accelerating voltage of 2.0 kV.

XRD

The XRD analysis was used to evaluate how 8-hydroxyquinoline interacts with the hydrogel biocomposites. It was performed on the hydrogel biocomposites at (Cu K_α radiation, λ=0.1546 nm) running at 45 kV and 40 mA using (PANalyticalX'Pert PRO), USA.

TEM

Transmission electron microscope was performed so as to evaluate the morphologies of rGO, 8-hydroxyquinoline, and

selected hydrogel biocomposites. TEM samples were prepared by dispersing the hydrogel biocomposites in deionized water. A drop of the solution was deposited onto copper grids, and the wet copper grids were allowed to dry on a filter paper at room temperature for 15 min prior to TEM analysis. TEM analysis was performed using JEM-1200EX, JEOL, Japan.

DSC

Thermal analysis was performed using the SDT Q600 DSC instrument (T.A. Instruments-Water LLC, Newcastle, DE 19720, USA). It was used to evaluate the thermal stability of the hydrogel biocomposites and 8-hydroxyquinoline. The DSC thermograph was recorded from 10 °C to 300 °C at a heating rate of 20 °C/min under a constant nitrogen flow (100 mL/min).

Results and discussion

FTIR

The FTIR spectrum for rGO-blank hydrogel composites exhibited absorption peaks for OH stretching at 3,346 cm^{-1}, NH stretching of amide at 3,182 cm^{-1}, C–H stretching at 2,931 cm^{-1}, C=O stretching of amide at 1,648 cm^{-1}, and CH_2 bending at 1,450 cm^{-1} (Fig. 1a). These characteristic peaks indicated the successful cross-linking of the acrylamides used for the preparation of the biocomposites.

The FTIR spectrum of rGO-1 showed absorption peaks at 3,333 cm^{-1} for OH stretching, NH stretching at 3,202 cm^{-1}, and at 2,931 cm^{-1} for CH stretching. C=O stretching of amide was visible at 1,657 cm^{-1}, NH bending of amide at 1,603 cm^{-1}, CH_2 bending at 1,439 cm^{-1}, and CH_3 bending at 1,347 cm^{-1}. Glycosidic C–O–C absorption peak was very outstanding at 1,160 cm^{-1}, which confirmed the successful cross-linking of WPI with acrylamide in the hydrogel biocomposite network (Fig. 1b).

FTIR spectrum (Fig. 1c) of rGO exhibited C=O carbonyl stretching at 1,727 cm^{-1}, C=C aromatic ring stretching absorption peak at 1,550 cm^{-1}, and C–O stretching vibration at 1,049 cm^{-1}, confirming the compound [33].

The FTIR spectrum for rGO-2 displayed absorption peaks for OH stretching at 3,338 cm^{-1}, NH stretching of amide at 3,195 cm^{-1}, CH stretching at 2,926 and 2,852 cm^{-1}, C=C stretching at 1,658 cm^{-1}, OH bending of carboxylic acid from rGO at 1,453 cm^{-1}, and C–O stretching at 1,397 cm^{-1}. C=O stretching for rGO was visible at 1,738 cm^{-1} which further confirmed the presence of rGO in the biocomposites. Glycosidic C–O–C absorption peak from WPI was visible at 1,167 cm^{-1}. This confirmed the presence and interaction of GO and WPI with the polymer chain (Fig. 1d).

Fig. 1 **a** FTIR spectrum of rGO-blank. **b** FTIR spectrum rGO-1. **c** FTIR spectrum of rGO. **d** FTIR spectrum of rGO-2. **e** FTIR spectrum of rGO-3. **f** FITR spectrum of 8-hydroxyquinoline. **g** FTIR spectrum of drug-loaded rGO-1

The FTIR spectrum for rGO-3 displayed absorption peaks for OH stretching at 3,338, NH stretching of amide at 3,182 cm^{-1}, CH stretching at 2,933 and 2,866 cm^{-1}; C=O stretching from rGO was visible at 1,739 cm^{-1} and C=C stretching at 1,652 cm^{-1}, and OH bending of carboxylic acid from rGO was visible at 1,445 cm^{-1} and 1,416 cm^{-1} respectively. This confirmed the presence and interaction of rGO with the polymer chain (Fig. 1e).

FTIR spectrum for 8-hydroxyquinoline displayed absorption peaks for C–N at 1,322 cm^{-1}, OH at 3,315 cm^{-1}, and C=C aromatic stretching at 1,474 cm^{-1}. C–O stretching vibration was visible at 1,586 cm^{-1} and C=N stretching at 1,641 cm^{-1} which confirmed the compound [32] (Fig. 1f).

FTIR spectrum for rGO-1 hydrogel biocomposite encapsulated with 8-hydroxyquinoline displayed absorption peaks for OH stretching at 3,338 cm^{-1}, NH stretching at 3,189 cm^{-1}, CH stretching at 2,927 cm^{-1}, C=O stretching of amide at 1,652 cm^{-1}, NH bending of amide at 1,603 cm^{-1}, CH_2 bending at 1,439 cm^{-1}, and CH_3 bending at 1,347 cm^{-1}, C–N stretching at 1,309 cm^{-1}, and glycosidic C–O–C absorption peak was very outstanding at 1,173 cm^{-1}. The absorption peaks confirmed the presence of WPI and 8-hydroxyquinoline in the hydrogel (Fig. 1g).

TEM

The surface morphologies of the hydrogel biocomposites were studied using TEM. rGO-blank exhibited thread-like amorphous morphology at selected magnification (Fig. 2a). rGO-3 exhibited a combination of star-shaped, folded, and thread-like morphologies (Fig. 2b). The folded morphology is attributed to the thermal reduction of GO to rGO, and the thread-like morphology is due to the cross-linking of acrylamide, methylenebisacrylamide, and TMEDA. TEM images of rGO-3 encapsulated with 8-hydroxyquinoline displayed spherical morphology as shown in (Fig. 2c). rGO exhibited a folded morphology (Fig. 2d) with wrinkles which further confirmed the compound [34, 35].

SEM

The surface morphologies of the prepared hydrogel biocomposites, partially rGO and 8-hydroxyquinoline were studied at selected magnifications. 8-Hydroxyquinoline exhibited a coarse surface with dot-shaped morphology at different magnifications which is attributed to its crystalline nature (Fig. 3a). rGO-blank hydrogel biocomposite displayed an irregular pattern of semi-coarse surface with spherically

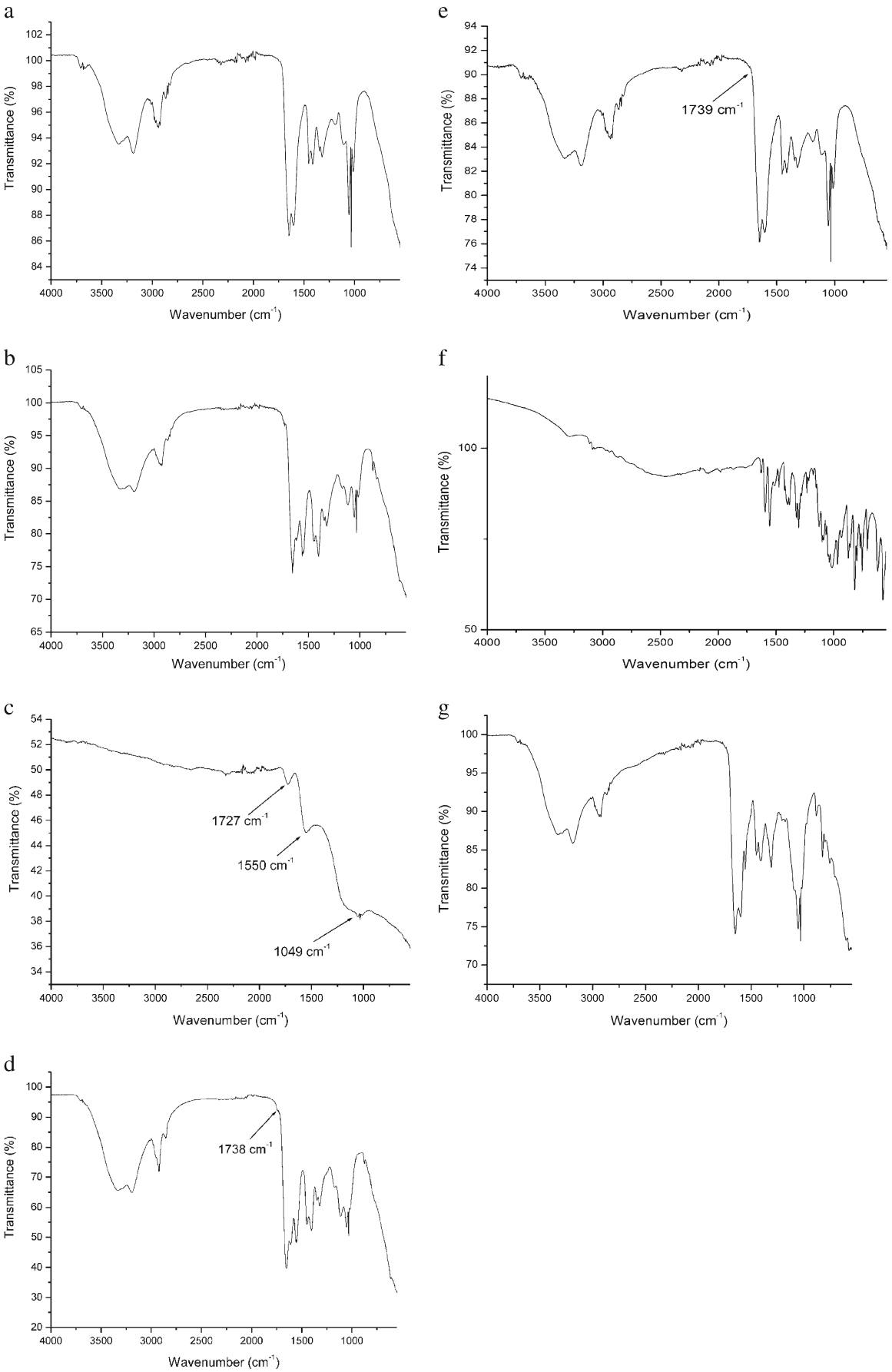
a
Transmittance (%)
Wavenumber (cm-1)
e
1739 cm-1
b
f
c
1727 cm-1
1550 cm-1
1049 cm-1
g
d
1738 cm-1

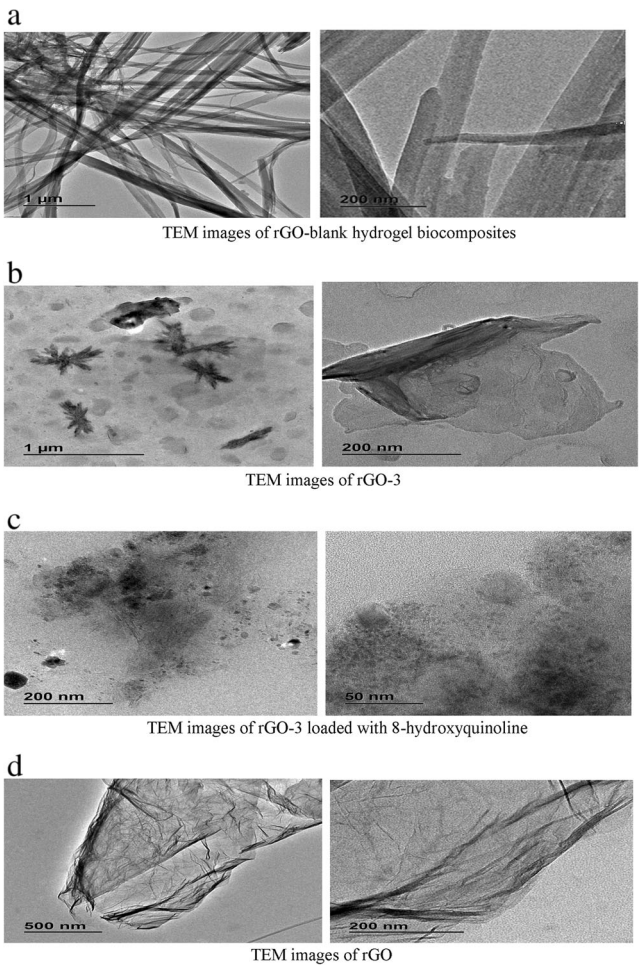

Fig. 2 **a** TEM images of rGO-blank hydrogel biocomposites. **b** TEM images of rGO-3. **c** TEM images of rGO-3 loaded with 8-hydroxyquinoline. **d** TEM images of rGO

shaped morphology which is attributed to the low degree of cross-linking. The surface was not as coarse as other hydrogel biocomposites that were cross-linked with WPI and had partially rGO in their network (Fig. 3b). rGO-1 hydrogel biocomposite displayed a uniform spherically coral-shaped morphology which is because of an increase in the degree of cross-linking (Fig. 3c). rGO-2 hydrogel biocomposite exhibited an irregular folded topologies which is because of the presence of partially rGO and WPI. This further confirms the higher degree of cross-linking when compared with the other hydrogel biocomposites (Fig. 3d). rGO-3 hydrogel biocomposite exhibited folded topologies which are of reduced degree when compared with rGO-2, and this is because of the absence of WPI (Fig. 3e). rGO-2 hydrogel biocomposite loaded with 8-hydroxyquinoline displayed a combination of irregular folded topologies and dot-shaped morphology which have been found in this study to be the characteristic features of rGO-2 and 8-hydroxyquinoline, respectively (Fig. 3f). This further confirmed the successful encapsulation of 8-hydroxyquinoline unto the hydrogel biocomposites. The digital photographs for the hydrogel biocomposites are shown in Fig. 3g.

XRD

XRD was used to evaluate the diffraction pattern of the hydrogel composites before and after encapsulation with 8-hydroxyquinoline. The diffraction pattern for rGO-blank was found to be broad due to the copolymerization reaction and its amorphous nature. Its characteristic peaks were found at $2\theta = 22.73°$, 28.20°, 31.96°, and 42.75°. The peaks for rGO-1 were broad and visible at $2\theta = 23.40°$ and 42.76° (Fig. 4a). rGO-2 and rGO-3 hydrogel biocomposites exhibited broad peaks at $2\theta = 23.05°$ and 23.07°, respectively (Fig. 4b). The characteristic peaks for rGO was not found, and this could be a result of the amorphous nature of the hydrogels. 8-Hydroxyquinoline exhibited sharp peaks due to its crystalline nature at $2\theta = 25.29$, 26.48, 27.85, 32.13, and 43.10, and these peaks were not seen in the hydrogel -loaded with 8-hydroxyquinoline (rGO-1) (Fig. 4c). The absence of the peaks for 8-hydroxyquinoline in the hydrogel-loaded 8-hydroxyquinoline suggests it was molecularly dispersed in the hydrogel network. The broad peaks confirmed the amorphous nature of the biocomposites. XRD analysis did not give much information, but it only confirmed the amorphous nature of the hydrogel biocomposites.

DSC analysis

The thermal stability, glass transition temperature, and the homogeneity of the hydrogel biocomposites and 8-hydroxyquinoline were studied using DSC. All the hydrogel biocomposites exhibited wide and broad endothermic peaks which can be attributed to the broad temperature range used. rGO-3 exhibited wide endothermic peak at 108 °C and a small endothermic peak at 195 °C (Fig. 5a). rGO-2 displayed a wide endothermic peak at 103 °C (Fig. 5a) whereas the rGO-blank exhibited wide endothermic peak at 145 and a small endothermic peak 200 °C (Fig. 5b). rGO-1 loaded with 8-hydroquinoline exhibited endothermic peaks at 89, 90, and 116 °C (Fig. 5a). 8-Hydroxyquinoline exhibited characteristic endothermic peaks at 138, 181, and 192 °C (Fig. 5c). These characteristics peaks were not found in the DSC thermograph of rGO-1 loaded with for 8-hydroxyquinoline, indicating that 8-hydroxyquinoline was molecularly dispersed in the hydrogel (Fig. 5a). To investigate the interaction of rGO with the polymer network, DSC analysis was also used to determine the glass transition temperature of the hydrogel biocomposites. The glass transition temperature (Tg) for rGO-1 biocomposites was 68.96 °C while rGO-3 biocomposites exhibited Tg at 81.72 °C. This indicated an increase from 68.96 to 81.72 °C when the rGO concentration increased from 0 to 0.007 g. The biocomposite containing WPI and rGO displayed Tg at 83.29 °C. This suggests that the

presence of natural polymer and rGO in the hydrogel network influenced the Tg of the biocomposites. The DSC results confirmed good dispersion of rGO in hydrogel network and a strong interaction between rGO and the new polymer chain [36, 37].

Swelling studies

Swelling property is important in biomedical application because drug release and the mechanism of drug release occur when diffusion of the drug is faster than the hydrogel swelling [38]. Equilibrium swelling studies of the dried hydrogel biocomposites were performed at ambient temperature over a period of 24 h. Selected buffer solution (pH 1.2, 7.4, and 10) simulating gastric juice, intestinal fluid, and basic pH, respectively, were used. Swelling ability of hydrogel biocomposites depends on various factors, such as the hydrophilic nature of the polymers, network density, the nature of solvent, and polymer solvent interaction [39]. rGO-2 hydrogel biocomposite exhibited the highest swelling ratio while

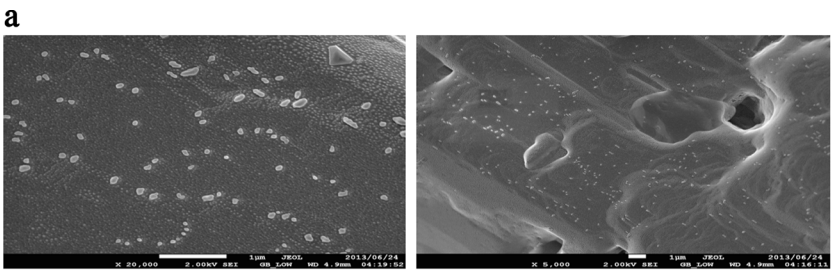

SEM images for 8-hydroxyquinoline

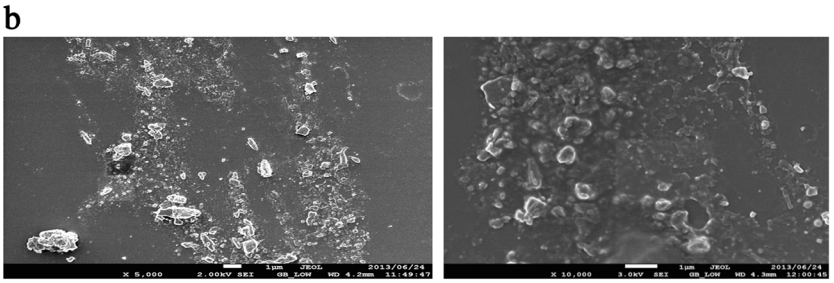

SEM images of rGO-blank

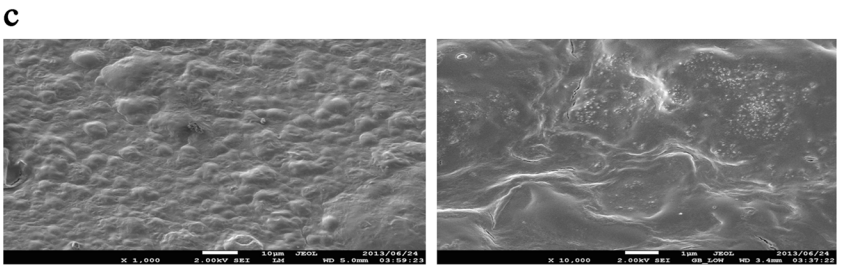

SEM images of rGO-1

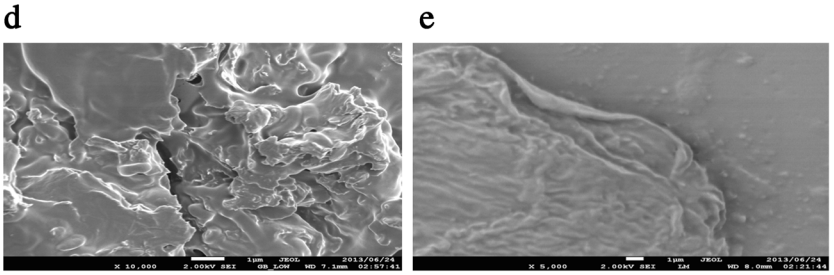

SEM image of rGO-2 SEM image of rGO-3

Fig. 3 **a** SEM images for 8-hydroxyquinoline. **b** SEM images of rGO-blank. **c** SEM images of rGO-1. **d** SEM images of rGO-2. **e** SEM images of rGO-3. **f** SEM images of rGO-1 loaded with 8-hydroxyquinoline. **g** Photograph of rGO-hydrogel biocomposites (**a**), rGO-1 (**b**), rGO-blank, and (**c**) rGO-3

f

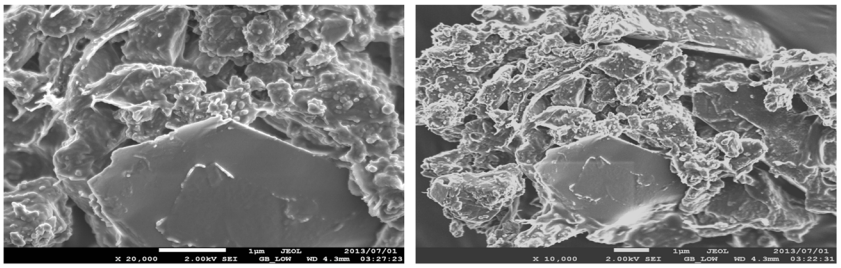

SEM images of rGO-1 loaded with 8-hydroxyquinoline

g

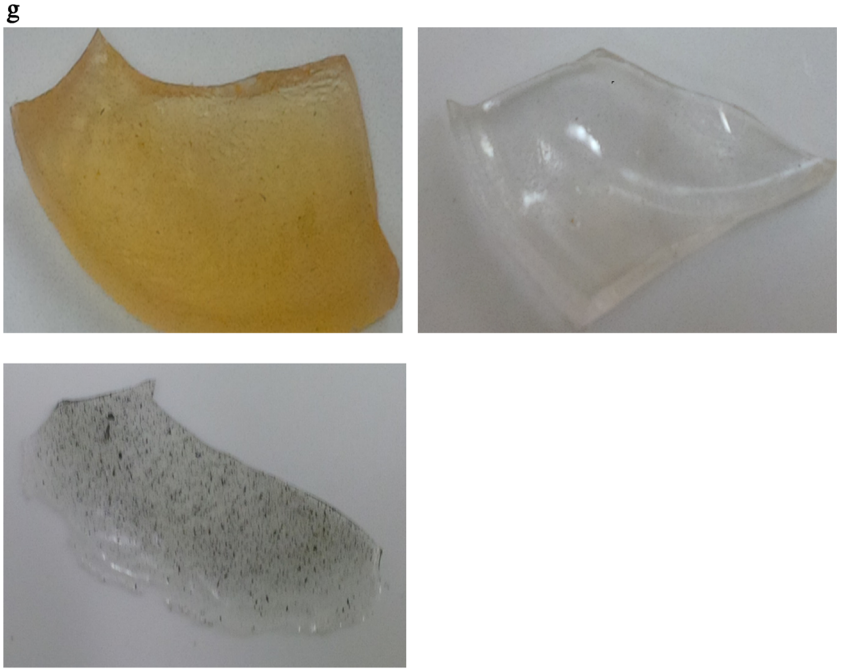

Photograph of rGO-hydrogel biocomposites (a) rGO-1 (b) rGO-blank (c) rGO-3

Fig. 3 (continued)

rGO-3 exhibited the lowest swelling ratio in the selected pH values. rGO-3 low swelling ratio is attributed to the reduced amount of hydrophilic functionalities on the surface of rGO used in the biocomposite. At pH values of 1.2, 7.4, and 10, rGO-2 hydrogel biocomposite exhibited the highest swelling ratio. This suggests that the swelling ratio of the hydrogel biocomposite increased with the addition of WPI, a natural polymer, and rGO. WPI and rGO contain hydrophilic groups, such as −OH, −CONH–, $-CONH_2$, −COOH,$–SO_3H$, and –COOH, −OH, −C–O–C–, respectively. Addition of WPI and rGO contribute to an increase in the density of hydrophilic groups which results in a high degree of water sorption and swelling ratio. The swelling ability of the hydrogel biocomposites were reduced at pH values 1.2 and increased at pH 7.4. At acidic pH, most of the carboxylate anions on rGO and the polymer network were protonated, and as such, anion–anion repulsive forces were eliminated, resulting in a decreased swelling ratio. At pH 7.4, the carboxylate groups were ionized, resulting in mutual repulsion between the carboxylate groups, and this increased swelling ability of the hydrogels. At basic pH of 10, the increase in swelling ratio was greater than at pH 1.2 because of the repulsion between the carboxyl groups which renders the network hydrophilic whereas, at pH 1.2, anion–anion repulsive forces reduced the degree of water sorption into the biocomposite network. The results obtained from the swelling analysis indicated that these biocomposites are potential targeted drug delivery systems that can be used to deliver drugs to the intestine.

The swelling ratios (SR) of the hydrogel biocomposites were examined after every 30 min at pH values of 1.2, 7.4, and 10. The solvent diffusion and polymer matrix relaxation effect were analyzed by examining the exponent n from [40] Eq. 5.

$$M_t/M_\infty = Kt^n \tag{5}$$

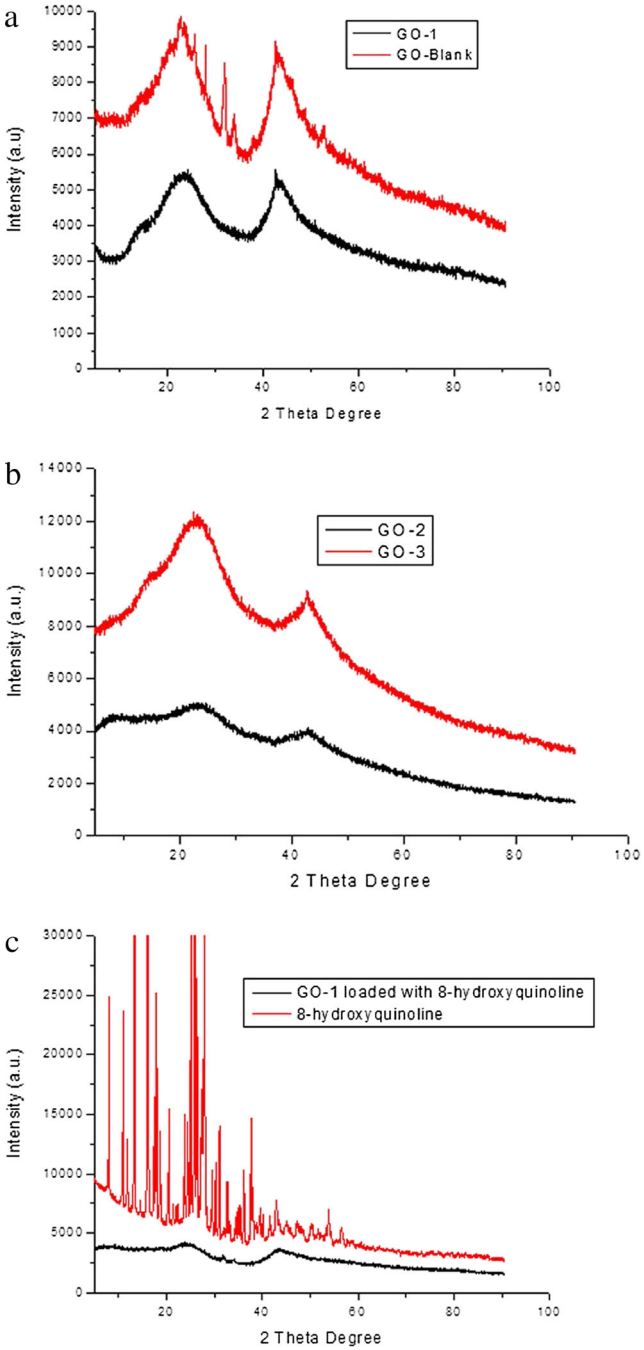

Fig. 4 **a** XRD graphs for rGO-blank and rGO-1. **b** XRD graphs for rGO and rGO-3. **c** XRD graphs for rGO and 8-hydroxyquinoline

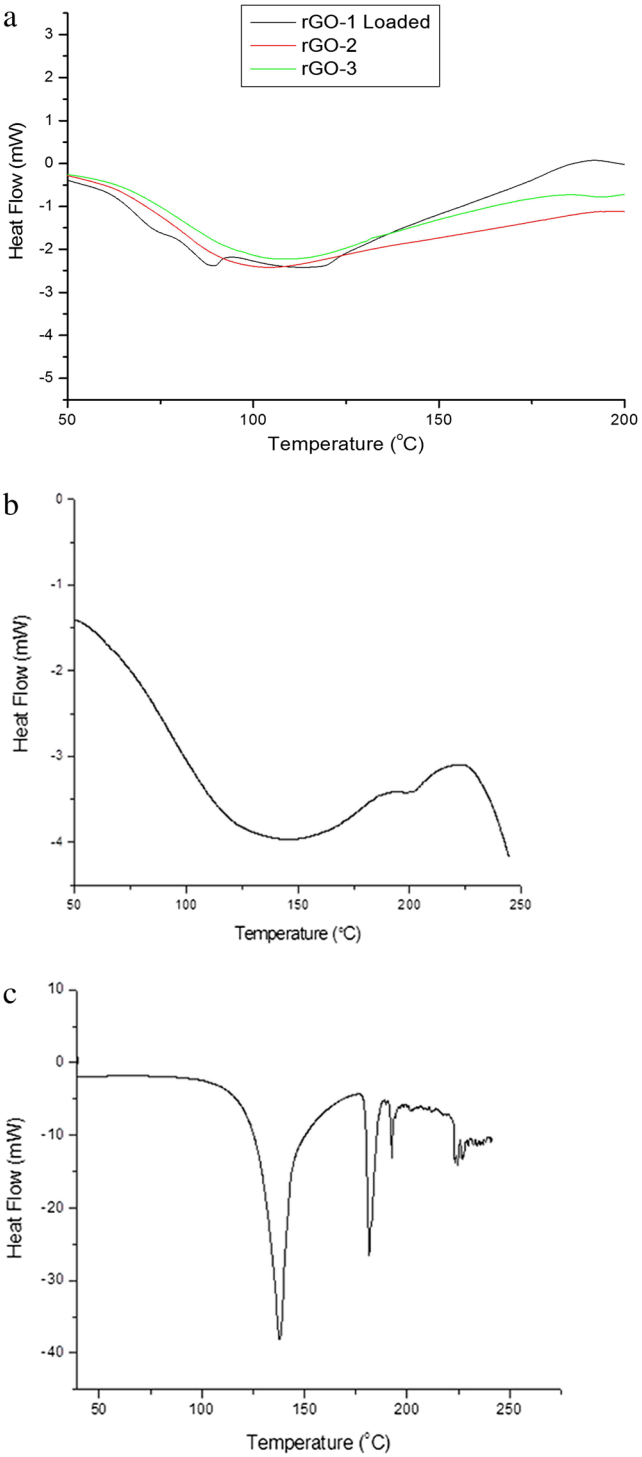

Fig. 5 **a** DSC graphs of rGO-2, rGO-3, and rGO-1 loaded with 8-hydroxyquinoline. **b** DSC graph for rGO-blank. **c** DSC graph of 8-hydroxyquinoline

Where M_t and M_∞ are the weight of the hydrogel biocomposite at time t and at equilibrium, respectively, K is the diffusion constant of water into the hydrogel network, and n is the diffusion exponent. When $n=0.5$, it indicates a case I which is a perfect Fickian process, in which the rate of network relaxation is faster than the rate of diffusion. When $n=1.0$, it indicates a non-Fickian diffusion where water transport is controlled and the rate of diffusion is faster than the network relaxation. When $0.5<n<1.0$, it indicates that the rate of penetrant mobility and segmental relaxation are comparable [40]. The swelling exponent n was determined from the slope of the graph of $Ln\ M_t/M_\infty$ versus $Ln\ t$ for swelling ratio of 60 % over a period of 6 h because more than 60 % swelling ratio was obtained during this period. The swelling exponent was

found to be in a range of between 0.51 and 0.78 at pH 1.2, 0.4 and 1.9 at pH 7.4, and between 0.44 and 0.6 at pH 10 with a coefficient of determination of 0.98–0.99, signifying good linearity (Table 2). The hydrogel diffusion coefficients were calculated [40] using Eq. 6:

$$S = 4\left[D/\pi r^2\right]^{1/2} t^{1/2} \quad (6)$$

where D, r, S, and t represent the diffusion coefficient of the hydrogel biocomposites, the radius of the hydrogel biocomposites, fractional swelling, and time, respectively. To further investigate the above findings, the diffusion coefficients of hydrogel biocomposites were evaluated from graphs of S versus $t^{1/2}$. They were calculated from the slopes. The diffusion coefficient was found to be highest in rGO-2 hydrogel biocomposite which exhibited the highest swelling ratio (Table 2). This result further confirmed that WPI and rGO influenced the degree of water sorption into the hydrogel network.

In vitro drug release studies

The drug release properties of the biocomposite were studied in buffer solutions of 1.2 and 7.4. 8-Hydroxyquinoline was selected as a drug of choice because of its solubility in water (10 g/100 mL), antimicrobial [41], antibacterial [42–44], and anticancer [45, 46] properties, and its ability to function as a transcription inhibitor. 8-Hydroxyquinoline was successfully encapsulated onto the hydrogel biocomposites in a range of 18–41 % (Table 1). Graphene-based hydrogel biocomposites are biocompatible [14] and also pH-sensitive, which qualify them as potential drug delivery systems. In vitro cumulative drug release profiles for the hydrogel biocomposites are shown in Fig. 6a and b. The rate of release of 8-hydroxyquinoline from the hydrogel biocomposites was influenced by the pH value. It was found that, in acidic buffer solution (pH 1.2), the release amount of 8-hydroxyquinoline was not more than 40 % after 24 h. At pH 7.4, the release amount increased significantly over 60 % after 6 h. This is attributed to the higher swelling ratio of the biocomposite at pH 7.4 when compared with pH 1.2. A research by Bai et al. [14] reported similar findings. This indicates that these biocomposites can bypass the acidity of gastric fluid without liberating substantial amounts of the loaded drug. rGO-2 hydrogel biocomposite released the drug faster than other hydrogels, and this is attributed to the hydrophilic groups on WPI and rGO, which increased the degree of water sorption and swelling ratio, thereby leading to increased

Table 2 Swelling data for the graphene containing hydrogel biocomposites

Hydrogel biocomposites	pH	R^2 (graph of Ln SR versus Ln time)	n	D (graph of SR versus $t^{1/2}$)	R^2
rGO-blank	1.2	0.98	0.78	0.33	0.98
rGO-1	1.2	0.98	0.67	1.59	0.99
rGO-2	1.2	0.99	0.54	1.40	0.99
rGO-3	1.2	0.98	0.67	1.59	0.99
rGO-blank	7.4	0.99	0.91	0.55	0.99
rGO-1	7.4	0.99	0.60	8.35	0.99
rGO-2	7.4	0.99	1.90	17.78	0.98
rGO-3	7.4	0.99	0.40	0.36	0.98
rGO-blank	10	0.99	0.44	0.41	0.98
rGO-1	10	0.99	0.60	1.87	0.98
rGO-2	10	0.99	0.46	1.66	0.98
rGO-3	10	0.99	0.54	0.99	0.41

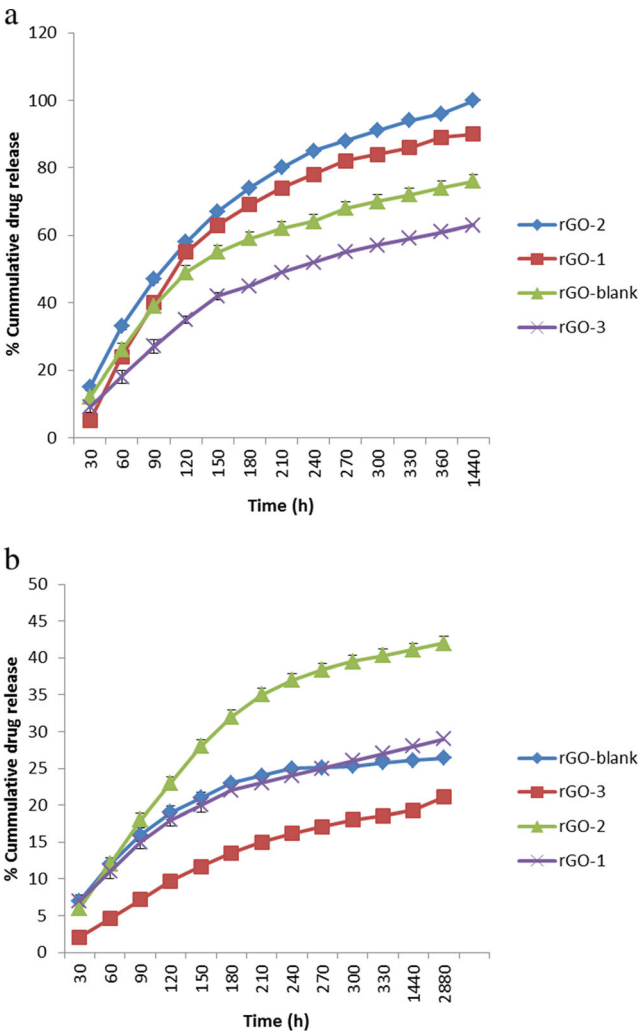

Fig. 6 **a** Plot of the cumulative release study of 8-hydroxyquinoline at pH 7.4. **b** Plot of the cumulative release study of 8-hydroxyquinoline at pH 1.2

rate of drug release. rGO-3 exhibited the slowest rate of drug release which is due to the reduced amount of hydrophilic groups. In order to explain the mechanism of drug release, Korsemeyer Peppas equation [40] was used (Eq. 7).

$$M_t/M_\infty = Kt^n \quad (7)$$

where M_t/M_∞ is the fraction of drug released at time t, K is a constant incorporating the structural and geometric characteristics of the hydrogel, and n is the release exponent, indicative of the mechanism of drug release. Diffusion exponent was estimated from the linear regression of Log M_t/M versus Log t for the first 60 % drug release. When n=0.5, it indicates a Fickian diffusion; when $0.5<n<1$, it indicates an anomalous or non-Fickian diffusion, which refers to a combination of diffusion- and erosion-controlled rate release. When n=1, it indicates case II, and when $n>1$, it indicates super case transport-II [47]. The plot of Log M_t/M_∞ against Log t was plotted for the experimental data according Eq. 4, and a good linearity was found, indicating that the Peppas's equation is applicable to the present systems. The release exponent n and the correlation coefficient R^2 for the hydrogel biocomposites were obtained, and they are listed in Table 3. At pH 1.2, rGO-1, rGO-2, and rGO-3 hydrogel biocomposites exhibited a release exponent of $0.5<n<1$, indicating a non-Fickian diffusion, which is a combination of diffusion- and erosion-controlled rate release. At pH 7.4, rGO-1, rGO-2, and rGO-3 exhibited release exponent values of 1.7, 0.98, and 0.82, respectively. This indicates a super case transport II and anomalous release mechanism, respectively. The results obtained suggest that the presence of rGO and WPI in the hydrogel network influenced the rate of drug release. The rate of release of 8-hydroxyquinoline from rGO-3 was delayed, and this can overcome the burst release problem of model drugs. rGO was found to exhibit a good drug-binding property for controlling the release rate of 8-hydroxyquinoline. Moreover, the drug release result was in good agreement with the effect of the pH on the swelling of hydrogel biocomposites as discussed in the previous section.

Table 3 The release exponents, n, and the correlation coefficient of the biocomposites

Hydrogel biocomposites	n (pH=1.2)	R^2 (pH=1.2)	n (pH=7.4)	R^2 (pH=7.4)
rGO-1	0.60	0.98	1.7	0.98
rGO-2	0.80	0.98	0.98	0.99
rGO-3	0.90	0.98	0.82	0.99

Conclusion

rGO hydrogel biocomposites were synthesized and characterized by SEM, XRD, and FTIR, which confirmed the successful incorporation of 8-hydroxyquinoline on to the hydrogels. The release behavior of 8-hydroxyquinoline and the swelling ratio of the biocomposites suggest that the biocomposites are pH-sensitive. At the preliminary investigation, rGO biocomposites were able to bypass the simulated acidity of the gastric juice without liberating substantial amount of loaded drug, and this indicates that rGO hydrogels can be used to deliver drug in the intestine with a controlled release mechanism and, hence, a potential targeted drug delivery system. This work proved that rGO hydrogel biocomposites exhibit a pH-induced drug release profile and that they can be used for loading and selectively releasing drugs at physiological pH values. Application may be exploited in order to expand the utilization of these systems in drug delivery applications. However, in vivo analysis is needed to confirm the results obtained in this research.

Acknowledgment The financial assistance of the South African National Research Foundation (NRF) towards this research is hereby acknowledged.

References

1. Geim AK, Novoselov KS (2007) The rise of graphene. Nat Mater 6:183
2. Park S, Ruoff RS (2009) Chemical methods for the production of graphene. Nat Nanotechnol 4:217
3. Geim AK (2009) Graphene: status and prospects. Science 324:1530
4. Tang L, Wang Y, Li Y, Feng H, Lu J, Li J (2009) Preparation, structure, and electrochemical properties of reduced graphene sheet films. Adv Funct Mater 19:2782
5. Wang C, Li D, Too CO, Wallace GG (2009) Electrochemical properties of graphene paper electrodes used in lithium batteries. Chem Mater 21:2604–2606
6. Huang X, Qi X, Boey F, Zhang H (2012) Critical review: graphene-based composites. Chem Soc Rev 41:666–686
7. Wang JJ, Zhu MY, Outlaw RA, Zhao X, Manos DM, Holloway BC, Mammana VP (2004) Free-standing subnanometer graphite sheet. Appl Phys Lett 85:1265–1267
8. Luo Z, Lu Y, Somers LA, Johnson AT (2009) High yield preparation of macroscopic graphene oxide membranes. J Am Chem Soc 131:898
9. Wang G, Wang B, Park J, Wang Y, Sun B, Yao J (2009) Highly efficient and large-scale synthesis of graphene by electrolytic exfoliation. Carbon 47:3242
10. Wang F, Graetz J, Morena MS, Ma C, Wu L (2011) Chemical distribution and bonding of lithium in intercalated graphite: identification with optimized electron energy loss spectroscopy. ACS Nano 5:1190–1197
11. Seger B, Kamat PV (2009) Electrocatalytically active graphene-platinum nanocomposites. Role of 2-D carbon support in PEM fuel cells. J Phys Chem C 113:7990–7995
12. Wu JB, Becerril HA, Bao ZN, Liu ZF, Chen YS, Peumans P (2008) Appl Phys Lett 92:263302

13. Shao Y, Wang J, Wu H, Liu J, Aksay IA, Lina Y (2010) Graphene based electrochemical sensors and biosensors: a review. Electroanal 22:1027–1036
14. Bai H, Li C, Wang X, Shi G (2010) A pH-sensitive graphene oxide composite hydrogel. Chem Commun 46:2376–2378
15. Sun S, Wu PA (2011) One-step strategy for thermal- and pH-responsive graphene oxide interpenetrating polymer hydrogel networks. J Mater Chem 21:4095–4097
16. Huang Y, Zenga M, Ren J, Wang J, Fan L, Xu Q (2012) Preparation and swelling properties of graphene oxide/poly(acrylic acid-co-acrylamide) super-absorbent hydrogel nanocomposites. Colloids and Surfaces A. Physicochem Eng Asp 401:97–106
17. Miao W, Shim G, Kang CM, Lee S, Choe YS, Choi H-G, Oh Y-K (2013) Cholesteryl hyaluronic acid-coated, reduced graphene oxide nanosheets for anti-cancer drug delivery. Biomaterials 34: 9638–9647
18. Wei G, Dong R, Wang D, Feng L, Dong S, Song A, Hao J (2014) Functional materials from the covalent modification of reduced graphene oxide and β-cyclodextrin as a drug delivery carrier. New J Chem 38:140–145
19. Wei G, Yan M, Dong R, Wang D, Zhou X, Chen J, Hao J (2012) Covalent modification of reduced graphene oxide by means of diazonium chemistry and use as a drug-delivery system. Chem Eur J 18: 14708–14716
20. Muller R, Keck C (2004) Challenges and solutions for the delivery of biotech drugs—a review of drug nanocrystal technology and lipid nanoparticles. J Biotechnol 113(1–3):151–170
21. Liu J, Gray WD, Davis ME, Luo Y (2012) Peptide- and saccharide-conjugated dendrimers for targeted drug delivery: a concise review. Interface Focus 2:307–324
22. Basu MK (1994) Liposomes in drug targeting. Biotechnol Genetic Eng Rev 12:383–408
23. Nasongkla N, Bey E, Ren J, Ai H, Khemtong C, Guthi JS, Chin S-F, Sherry AD, Boothman DA, Gao J (2006) Multifunctional polymeric micelles as cancer-targeted, MRI-ultrasensitive drug delivery systems. Nano Lett 6:2427–2430
24. Lamprecht A, Ubrich N, Yamamoto H, Scha¨ Fer U, Takeuchi H, Maincent P, Kawashima Y, Lehr C-M (2001) Biodegradable nanoparticles for targeted drug delivery in treatment of inflammatory bowel disease. J Pharmacol Exp Ther 299:775–781
25. Gu Z, Dang TT, Ma M, Tang BC, Cheng H, Jiang S, Dong Y, Zhang Y, Anderson DG (2013) Glucose-responsive microgels integrated with enzyme nanocapsules for closed-loop insulin delivery. ACS Nano 7:6758–6766
26. Unique nano carrier to target drug delivery to cancer cells." ScienceDaily. ScienceDaily, 28 October 2013. <www.sciencedaily.com/releases/2013/10/131028135039.htm. Accessed 10th February 2014
27. Researchers develop sticky nanoparticles to fight heart disease. http://www.rdmag.com/news/2014/02/researchers-develop-sticky-nanoparticles-fight-heart-disease, Accessed 18th February 2014
28. Ren K, Dusad A, Dong R, Quan L (2013) Albumin as a delivery carrier for rheumatoid arthritis. J Nano Med Nano Techol 4:4
29. Jonker A, Lowik DW, Van Hest JCM (2012) Peptide and protein-based hydrogels. Chem Mater 24:759–773
30. Shanshan LV, Cao YI, Hongbin LI (2012) Tandem modular protein-based hydrogels constructed using a novel two-component approach. Langmuir 28:2269–2274
31. Jayaramudu T, Raghavendra GM, Varaprasad K, Sadiku ER, Rajua KM (2013) Development of novel biodegradable Au nanocomposite hydrogels based on wheat: for inactivation of bacteria. Carbohydr Polym 92:2193–2200
32. Rajasekaran M, Anbusrinivasan P, Mojumdar SC (2010) Growth, spectral and thermal characterization of 8-hydroxyquinoline. J Therm Anal Calorim 100:827–830
33. Chen W, Yan L (2010) Preparation of graphene by a low-temperature thermal reduction at atmosphere. Nanoscale 2:559-563
34. Ju HM, Choi SH, Huh SH (2010) X-ray diffraction patterns of thermally-reduced graphenes. J Korean Phys Soc 57:1649–1652
35. Huh SH. Thermal reduction of graphene oxide, physics and applications of graphene experiments, http://www.intechopen.com/download/get/type/pdfs/id/15270, accessed 20th December 2013
36. Aldosari MA, Othman AA, Alsharaeh EH (2013) Synthesis and characterization of the *in situ* bulk polymerization of PMMA containing graphene sheets using microwave irradiation. Molecules 18: 3152–3167
37. Chen G, Qiao C, Xu J, Yao J (2014) Synthesis and characterization of reduced graphene oxide/gelatin composite films. Polym (Korea) 38: 484–490
38. Colombo P, Bettini R, Santi P, Ascentiis AD, Peppas NA (1996) Analysis of the swelling and release mechanisms from drug delivery systems with emphasis on drug solubility and water transport. J Control Release 39:231–237
39. Ottenbrite RM, Kinam P, Okano T (2010) Biomedical applications of hydrogels handbook. Springer, 4–8
40. Ritger P, Peppas NA (1987) Simple equation for description of solute release I. Fickian and non-Fickian release from non-swellable devices in the form of slabs, spheres, cylinders or discs. J Control Release 5: 23–36
41. Jeon JH, Lee CH, Lee SH (2009) Antimicrobial activities of 2-methyl-8-hydroxyquinoline and its derivatives against human intestinal bacteria. J Korean Soc Appl Biol Chem 52:202–205
42. Abuthahir SSS, Nasser AJA, Rajendran S, Brindha G (2014) Synthesis, spectral studies and antibacterial activities of 8-hydroxyquinoline derivatives and its metal complexes. Chem Sci Transf 3:303–313
43. Jeon JH, Lee CH, Lee HS, Gopalchari R, Dhar ML (1960) J Sci Ind Res 19C:233
44. Blunden SJ, Patel BN, Smith PJ, Sugavanam B (1987) Synthesis, ^{119}Sn NMR and Mössbauer studies and bioassay data of *O*-tricyclohexylstannyl derivatives of substituted 8-hydroxyquinolines. Appl Organomet Chem 1:241–244
45. Ogata A, Kaneko T (1944) J Pharm Soc Japan 11:246
46. Maggio GD, Ciaceri G (1955) Russ Clin Ter Sci Affin 54:217
47. Costa P, Lobo JMS (2001) Modeling and comparison of dissolution profiles. Eur J Pharm Sci 13:123–133